

Designer Magnetism in High Entropy Oxides

Alessandro R. Mazza¹, Elizabeth Skoropata¹, Yogesh Sharma^{1,2}, Jason Lapano¹, Thomas W. Heitmann³, Brianna L. Musico⁴, Veerle Keppens⁴, Zheng Gai⁵, John W. Freeland⁶, Timothy R. Charlton⁷, Matthew J. Brahle¹, Adriana Moreo^{1,8}, Elbio Dagotto^{1,8}, Thomas Z. Ward^{1,*}

¹Materials Science and Technology Division, Oak Ridge National Laboratory, Oak Ridge, Tennessee 37831, USA

²Center for Integrated Nanotechnologies, Los Alamos National Laboratory, Los Alamos, New Mexico 87545, USA

³University of Missouri Research Reactor, The University of Missouri, Columbia, Missouri 65211, USA

⁴Department of Materials Science and Engineering, University of Tennessee, Knoxville, Tennessee 37996-4545, USA

⁵Center for Nanophase Materials Sciences, Oak Ridge National Laboratory, Oak Ridge, Tennessee 37831, United States

⁶Advanced Photon Source, Argonne National Laboratory, Lemont, Illinois 60439, USA

⁷Neutron Science Division, Oak Ridge National Laboratory, Oak Ridge, Tennessee 37831, USA

⁸Department of Physics and Astronomy, University of Tennessee, Knoxville, TN 37996, USA

*email: wardtz@ornl.gov

Disorder can have a dominating influence on correlated and quantum materials leading to novel behaviors which have no clean limit counterparts. In magnetic systems, spin and exchange disorder can provide access to quantum criticality, frustration, and spin dynamics, but broad tunability of these responses and a deeper understanding of strong limit disorder is lacking. In this work, we demonstrate that high entropy oxides present an unexplored route to designing quantum materials in which the presence of strong local compositional disorder hosted on a positionally ordered lattice can be used to generate highly tunable emergent magnetic behaviors—from macroscopically ordered states to frustration-driven dynamic spin interactions. Single crystal $\text{La}(\text{Cr}_{0.2}\text{Mn}_{0.2}\text{Fe}_{0.2}\text{Co}_{0.2}\text{Ni}_{0.2})\text{O}_3$ films are used as a structurally uniform model system hosting a magnetic sublattice with massive microstate disorder in the form of site-to-site spin and exchange type inhomogeneity. A classical Heisenberg model is found to be sufficient to describe how compositionally disordered systems can paradoxically host long-range magnetic uniformity and demonstrates that balancing the populating elements based on their discrete quantum parameters can be used to give continuous control over ordering types and critical temperatures. Theory-guided experiments show that composite exchange values derived from the complex mix of microstate interactions can be used to design the required compositional parameters for a desired response. These predicted materials are synthesized and found to possess an incipient quantum critical point when magnetic ordering types are designed to be in direct competition; this leads to highly controllable exchange bias sensitivity in the monolithic single crystal films previously accessible only in intentionally designed bilayer heterojunctions.

I. INTRODUCTION

Magnetism is the most easily observable quantum phenomenon and is a cornerstone of technologies ranging from magnetic memory, to spintronics, to future quantum sensing and computing applications [1–4]. The type and strength of magnetic state in crystalline materials is dictated by discrete values, such as the number of unpaired electrons and type of magnetic exchange pathways populating the crystal lattice. The development of predictive design strategies aimed at tailoring functional magnetic responses is then entirely reliant on our ability to not only computationally forecast what parameters must be present on a lattice to generate a required magnetic behavior, but these parameters must also be translated into real materials through synthesis. This is fundamentally challenging, since direct continuously tunable control over spin (S) and magnetic exchange (J) values is needed to access a precisely defined parameter space; however, these values must be experimentally created using the limited set of spin active elements. There are several indirect methods used to influence magnetic responses in strongly correlated materials, such as where heteroepitaxial effects and defect engineering are commonly used to manipulate spin-coupled charge and orbital parameters [5–9]. Direct modification to the underlying S and J values using substitutional doping approaches are traditionally limited by thermodynamic processes during synthesis which can cause like elements to cluster or form secondary phases [10]. Thus, while substitutional doping promises the most direct route to accessing the magnetic parameters used in computational approaches, enthalpic effects during synthesis can drive element segregation which limits mixing and reduces the number of desired composite microstates that exist in well-mixed regions [11]. Recent developments in entropy-assisted synthesis provide a path to overcoming enthalpic effects and create well mixed systems [12].

By greatly increasing the number of elements present in a material during synthesis, it is possible for entropic effects to dominate during crystal formation [13,14]. The governing entropy ensures exceptional mixing, which maximizes the number of local microstates hosted on a lattice [15]. Increasing local disorder in entropy stabilized materials is linked to significant functional improvements in thermal transport [16,17], ionic conductivity [18,19], and catalytic responses [20,21] over less complex materials. Recent work has shown that this compositional disorder can be accommodated on ordered single crystalline lattices, which reduces the need to consider extrinsic parameters in computational models [22–25]. In this way, the effects of

known element-specific parameters and inter-atomic couplings can be microscopically mapped to materials of extraordinary compositional complexity to predict macroscopic collective behavior, and critically, these compositionally complex but structurally uniform crystals can be synthesized in the real world.

Unlike high entropy alloys built from metal-metal bonded elements [13,26], high entropy oxides give access to functionalities in covalent and ionic bonded materials. While the metal-bonded high entropy alloys are limited in their range of crystal structures, stability, and accessible magnetic interaction pallet, the addition of an anion sublattice enables a broad range of stable crystal structures and greater access to functional diversity [14,15]. Still, considering the sensitivity of spin behavior to bond angles and cation orbital filling in many oxide systems [27,28], it is surprising that high entropy oxides hosting high levels of compositional disorder have been reported to support signatures of long range magnetic ordering in both relatively simple rock salt lattices [29–31] and more complicated spinel [32] and perovskite [33,34] structures. In all cases, the mechanism of ordering must revolve around the type and strength of exchange couplings populating the lattices as a function of the elemental compositions. This is fundamentally different from the itinerant RKKY or dilute type magnetism observed in metal-metal bonded systems [13,35]. The addition of the anion sublattice in the high entropy oxides promises a greater diversity of magnetic interactions enabled by localized rather than delocalized electron coordination.

In this work, a range of single crystal entropy stabilized ABO_3 perovskite films are synthesized to probe how manipulating variances in site-to-site spin and exchange interactions influence magnetic behaviors. We explain how compositionally disordered systems can paradoxically host long-range magnetic uniformity and demonstrate that balancing the populating elements based on their discrete parameters can be used to give continuous control over ordering types and critical temperatures. A series of theory-guided experiments show that composite exchange values derived from the complex mix of microstate interactions can be used to design the required compositional parameters needed to stabilize macroscopic ferromagnetism (FM), antiferromagnetism (AFM), and to set critical temperatures across a continuum of values. Manipulating the S and J parameters through compositional ratio also provides access to an incipient quantum critical point (QCP) at an AFM to FM phase crossover, where the phases are shown to be in direct competition. We also discover that manipulating the local spin disorder can

be used to drive exchange bias behaviors in the monolithic single crystal films similar to that observed in AFM-FM bilayer heterojunctions; this provides important new insights into recent proposals that spin and exchange disorder can be the dominating factor in generating exchange bias responses [36].

II. RESULTS

$\text{La}(\text{Cr}_{0.2}\text{Mn}_{0.2}\text{Fe}_{0.2}\text{Co}_{0.2}\text{Ni}_{0.2})\text{O}_3$ (L5BO) is an ideal high entropy oxide system to examine the role of local magnetic disorder on the emergence of macroscopic magnetic behaviors. Structurally, this material possesses full mixing of the *B*-site cations while maintaining long-range single crystal lattice uniformity [25,34]. There also exists a large body of theoretical and experimental work on the parent compounds, LaCrO_3 , LaMnO_3 , LaFeO_3 , LaCoO_3 , and LaNiO_3 and a range of interfacial and co-doping studies that allow us insights into expected spin, charge, and oxygen mediated coupling types between each of the different *3d* transition metal cations [37–54]. Figure 1 provides relevant examples from literature of magnetic ordering types and transition temperatures for ternary and quaternary lanthanide transition metal oxides [55]. Of the 15 different materials, 8 are reported or expected to undergo AFM transitions with Neel temperatures within the range of 740 K to 160 K, while the remaining 7 have FM transitions with Curie temperatures within the range of 230 K to 50 K. From this, it is possible to extrapolate the

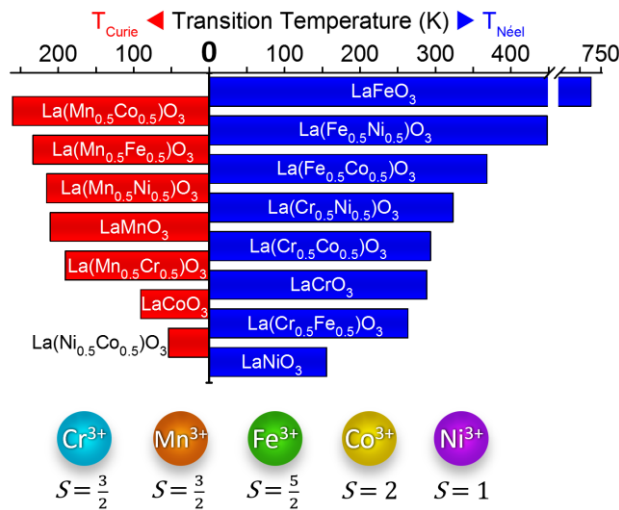


FIG. 1. Comparison of ABO_3 transition metal oxides' magnetic behaviors. Magnetic ordering type and transition temperatures for a range of lanthanide transition metal oxides show the wide range of functional phase space accessible by changing the *B*-site cation. Red denotes ferromagnets and blue denotes antiferromagnets. Examples of the discrete charge and spin states for representative *3d* transition metal cations are provided for reference.

local (first nearest-neighbor) exchange interactions and energies that drive the macroscopic magnetic responses observed in each of these relatively simple parent materials [55].

In the L5BO system, all these 15 exchange interaction types are present. The randomly placed cations on the *B*-site sublattice create a locally chaotic environment populated by multiple spin values connected by both AFM and FM exchange couplings of varying magnitude and sign depending on the neighboring elements. This creates an extraordinary amount of local site-to-site magnetic disorder on a structurally ordered lattice. The ordering allows these complex magnetic interactions to be modeled classically for a square lattice by considering the range of possible exchange interactions distributed across the lattice [56–58]. This creates a diverse and complicated array of possible exchange coupling terms and local spin environments. Allowing only for 3⁺ charge states of each of the constituent *B*-site elements in L5BO, a calculation of the magnetic order parameter can be found by considering all possible microstates in a random distribution on the perovskite lattice. For the theoretical prediction of the magnetic behavior corresponding to L5BO, a Monte Carlo study is performed on a cubic lattice using the classical Heisenberg model defined as:

$$H = \sum_{\langle ij \rangle} J_{ij} \mathbf{S}_i \cdot \mathbf{S}_j$$

\mathbf{S}_i are classical spins of different magnitudes depending on which transition metal element is placed at site *i*. The symbol $\langle ij \rangle$ refers to nearest-neighbor (NN) sites. For the location of the spins, a random distribution based on a probability is used such that each element covers 20% of the finite clusters employed for the simulation [55]. For the magnitudes of the spin of each transition metal ion, the values taken are $S=5/2$ for Fe, $S=2$ for Co, $S=3/2$ for Cr and Mn, and $S=1$ for Ni. While there are possible uncertainties with regards to what specific spin should be assigned to some elements in the 20% *B*-site occupancy perovskite, for the theory results described below one of the key factors determining the overall dominance of AFM is that Fe³⁺ has antiferromagnetic tendencies in 4 of its 5 bonds *i.e.*, in Fe-O-Fe, Fe-O-Cr, Fe-O-Co, and Fe-O-Ni, where O is the bond oxygen. Fe³⁺ is safely assigned a value $S=5/2$ because it corresponds to one electron per 3*d* orbital (3*d*⁵) which maximizes the spin due to the strong Hund coupling of Fe.

The spin values are relatively easy to predict in magnitude, but the values J_{ij} are more difficult because there are 15 possible combinations X-O-Y (with X,Y=Cr, Mn, Fe, Co, Ni). While a simple summary of critical temperatures of parent materials is given in Fig. 1, a detailed analysis along with the existing experimental literature used to deduce J_{ij} can be found in supplemental material [55]. For the 5 X-O-X cases, this task is simplified, because the critical temperatures of the LaXO_3 materials can be directly related to their superexchange J , positive or negative depending on whether the order is AFM or FM. For the other 10 X-O-Y ($X \neq Y$) cases, finding J_{ij} is more challenging and critical temperatures for 50% mixes $\text{LaX}_{0.5}\text{Y}_{0.5}\text{O}_3$, superlattices $\text{LaXO}_3\text{-LaYO}_3$, or in some cases interpolations between existing data are used. The summary of this effort is the following. There are 8 AFM $J_{ij} > 0$ and 7 FM $J_{ij} < 0$ commensurate with Fig. 1, suggesting a fine balance between the two tendencies. However, the actual magnitudes of the AFM set $J_{ij} > 0$ are considerably stronger than those with FM character. Moreover, as explained above, the largest spin $S=5/2$ for Fe^{3+} plays an important role for the AFM dominance. The FM tendencies are primarily driven by the links containing Mn.

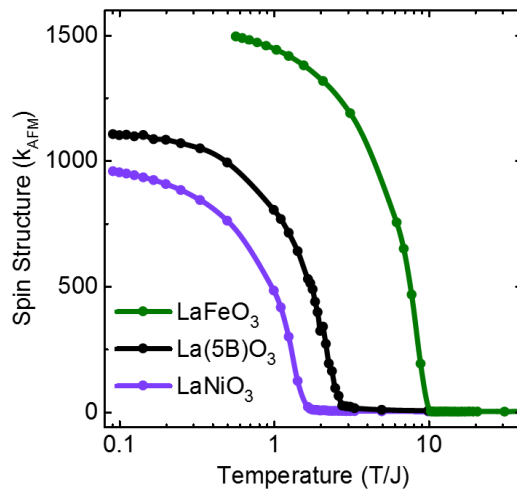


FIG. 2. Comparison of calculated spin structure factor $S(k_{AFM})$ at wavevector $k_{AFM} = (\pi, \pi, \pi)$ vs temperature, T/J , where J is taken as 82 K, for LaFeO_3 , LaNiO_3 , and entropy-stabilized $\text{La}(\text{Cr}_{0.2}\text{Mn}_{0.2}\text{Fe}_{0.2}\text{Co}_{0.2}\text{Ni}_{0.2})\text{O}_3$. The model matches known transition behaviors for the simple ternary compounds and predicts a G-type antiferromagnetic ordering in the L5BO system with a $T_N \approx 210$ K.

The results shown in Fig. 2 use $10 \times 10 \times 10$ clusters, with periodic boundary conditions in all directions, and the Monte Carlo simulation technique to model expected magnetic responses of the L5BO system and two related and well-studied ternary systems. An annealing process from high temperature (i.e., slow cooling) is employed to avoid being trapped into metastable

states. Some of the simulations are repeated using $12 \times 12 \times 12$ clusters and the results for critical temperatures do not change appreciably considering the uncertainties in superexchange values used. Moreover, the Monte Carlo results shown correspond to averages over 5 independent random distributions of spins, but self-averaging renders the 5 results nearly identical within the accuracy needed. This comparison provides an interesting point, by suggesting it is this average which dictates the predominant order type in the film. After equilibrium, Monte Carlo is used to measure the standard spin-spin correlations $\langle \mathbf{S}_i \cdot \mathbf{S}_j \rangle$ in real space at all distances and from them calculate the spin structure factor $S(\mathbf{k})$ by Fourier transform:

$$S(\mathbf{k}) = \frac{1}{N} \sum_{i,j} \langle \mathbf{S}_i \cdot \mathbf{S}_j \rangle e^{i\mathbf{k} \cdot (\mathbf{r}_i - \mathbf{r}_j)}$$

\mathbf{r}_i is the vector position in the cubic lattice of site i . Among allowed momenta, we searched for the one that maximized $S(\mathbf{k})$. In all simulations of the equiatomic B -site perovskite using the couplings and spins discussed above, the dominant peak in $S(\mathbf{k})$ is always found to be located at (π, π, π) , i.e., in the AFM position. Despite the many FM couplings used, no peak at $(0,0,0)$ is detected. Typical results are presented in Fig. 2 where $S(k_{AFM})$, with $k_{AFM} = (\pi, \pi, \pi)$, is shown as a function of temperature for the pure 100% Fe-O-Fe case (with the largest spin), the 100% Ni-O-Ni (with the smallest spin), and the 20% equiatomic B -site populated L5BO. Considering that $T_N = 740$ K for pure LaFeO_3 , this establishes the scale J in Fig. 2 to be ≈ 82 K after rescaling of existing Monte Carlo results, giving a theoretical prediction that L5BO is AFM with $T_N \approx 210$ K [59].

Experimentally, neutron diffraction confirms that this complex mix of local microstates creates long-range magnetic ordering in both the bulk powder ceramic and single crystal thin film forms (Fig. 3(a)-(b)). These results are presented considering the cubic Miller indices of the film, where the $(0\ 0\ 1)$ peak refers to the structural and temperature-independent feature in the powder diffraction, and the $(\frac{1}{2}\ \frac{1}{2}\ \frac{1}{2})$ peak is an AFM Bragg peak occurring only below T_N . The temperature dependence of the $(\frac{1}{2}\ \frac{1}{2}\ \frac{1}{2})$ peak of the L5BO in polycrystalline form provides an order parameter that shows an onset of AFM occurring between the measurements taken at 300 K and 150 K, which is consistent with Mössbauer results in previous studies of L5BO powder produced by spray pyrolysis [33]. Since single crystals may help preclude possible extrinsic contributions related to complexity of grain size, surface effects, and inhomogeneous mixing of

constituents, neutron diffraction is also performed on single crystal films grown on near lattice matched LSAT substrates to allow the film to maintain a nearly cubic structure such as that used in the Monte Carlo simulations [34,55]. The temperature-dependent evolution of the $(\frac{1}{2} \frac{1}{2} \frac{1}{2})$ peak is shown in Fig. 3(b) and demonstrates a clear G-type AFM transition in the L5BO film. While the exact onset temperature is somewhat hidden by the substrate background signal at higher temperatures, the onset trend agrees with irreversibility in temperature-dependent magnetization in the field cooled vs zero field cooled SQUID magnetometry results, implying that the Neel temperature occurs near 180 K [55].

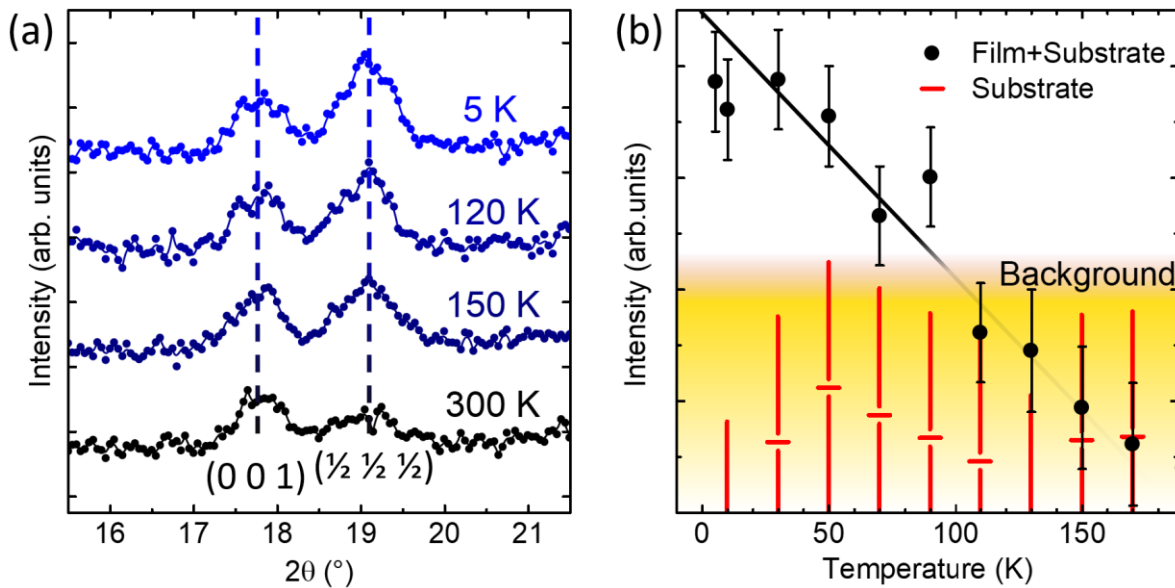


FIG. 3. Observation of G-type antiferromagnetic ordering in L5BO bulk and film. (a) Temperature dependent neutron diffraction of bulk polycrystalline L5BO sample shows the $(\frac{1}{2} \frac{1}{2} \frac{1}{2})$ peak emerge and increase in intensity with decreasing temperature which is consistent with the onset G-type antiferromagnetism. No other temperature dependent peaks were observed and the structural $(0 0 1)$ peak is included for reference. (b) Neutron diffraction data taken for the order parameter of the $(\frac{1}{2} \frac{1}{2} \frac{1}{2})$ peak in a L5BO single crystal film on an LSAT substrate shows the onset of magnetic order emerging near the predicted Neel temperature.

The AFM found in simulation appears percolated rather than isolated, which matches the long-range AFM order observed in experiment. Only a single transition temperature is observed at $T_N \approx 180$ K, which remarkably matches the Heisenberg model's prediction. This shows that it is possible to design critical temperature and macroscopic ordering type by intelligently selecting a set of elements based on the average of their fundamental S and J into account. This gives access to continuously tunable magnetic phase spaces that are not accessible using less complex compositions. However, the uniformly percolated AFM state matching the Heisenberg model in the case of an average spin or exchange interaction over the whole lattice described above gives

the false impression of being a "standard" AFM from the macroscopic perspective. In the equiatomic L5BO system, the FM bonds account for 40% of the total exchange interaction strength. This means that the AFM order dominates the FM order only by a narrow margin. This leaves the questions as to why FM is not more strongly observed considering that there are so many FM links. To understand how local spin and exchange disorder lead to this behavior, it is informative to consider the microscopic landscape by considering the local distribution of FM and AFM connections within the $10 \times 10 \times 10$ simulation.

Fig. 4(a) presents a section of a typical 10×10 slice of the simulation showing the sign of the thermalized NN spin-spin correlations at each link after equilibrium. Here, regions of ferromagnetically coupled neighbors are clearly observed embedded in a continuous antiferromagnetic matrix. These FM regions appear at the same critical temperature as AFM order but are not coherently coupled among each other, which prevents percolation of the FM state. This intrinsic frustration in the L5BO magnetic lattice is highlighted by the non-collinearity of the equilibrated spins; and while AFM order dominates, the average of the parent oxides does not complete the story. When considering the distribution of superexchanges prior to equilibrium or considering only the inputs for nearest neighbor interactions produced from literature $J(S_i \cdot S_j)$, this imbalance shows that at higher temperature one might expect the FM character of the crystal

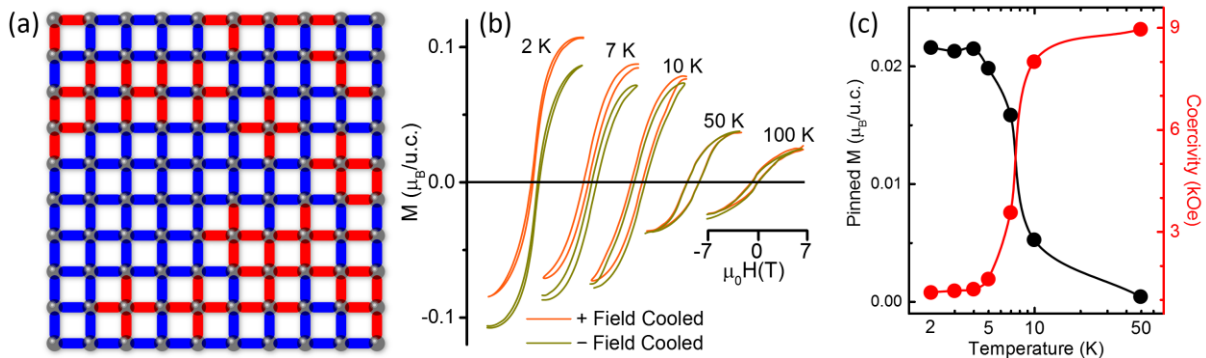


FIG. 4. Influence of frustrated and unpercolated ferromagnetic coupling. (a) Typical Monte Carlo simulation equilibrated snapshot of a 10×10 slice from the $10 \times 10 \times 10$ cube of L5BO system show that unpercolated FM clusters can persist in a percolated AFM matrix at low temperature. Red indicates links with a positive nearest neighbor $S_i \cdot S_j$ which are mainly FM links in equilibrium low temperature while blue represent AFM linkages. (b) Field biased magnetization loops taken across a range of temperatures after field cooling under ± 7 T, show the pinned FM moments driving a vertical shift in the field biased loops below the blocking temperature, T_B , consistent with transition to a low temperature AFM phase populated by scattered unpercolated FM exchange sites. (c) Summary of experimentally obtained magnetization behaviors of L5BO film subjected to field cooling from 300 K demonstrates the manifestation of low temperature hindered percolation of the FM clusters. Magnetic pinning increases and coercivity decreases as the AFM phase hardens through T_B .

to play more of a visible role [55]. As the zero-energy state is approached upon cooling, the AFM becomes much more dominant. That means that there should exist some relatively small external perturbation strength, or small energy scale, above which the FM phase may percolate within the AFM matrix and below which the FM regions remain locally isolated. The AFM state is thus predicted to be fragile, and at the verge of switching to a ferromagnet. Experimentally, this can be tested by applying a magnetic field strong enough to saturate the FM regions and then field cooling to a temperature below the blocking temperature (T_B) of the AFM region [36,60]. This effectively locks-in pockets of aligned moments and creates a surplus magnetization that is observable as a vertical shift in any field-dependent magnetization loops [61]. This vertical shift results from pinning of the uncompensated and FM spins and is distinctly different from horizontal loop shifts associated with magnetic exchange bias resulting from coupled AFM-FM systems where a fully formed FM component can overcome the interfacial energy and rotate fully [62,63]. Fig. 4(b) shows examples of field-dependent magnetization loops at different temperatures after field cooling under ± 7 T and are summarized in Fig. 4(c). As temperature decreases, the coercive field drops. This indicates the FM clusters effectively behave as single domains rotating freely with field as in a superparamagnetic regime—suggesting the unpinned moments are isolated at low temperature. The drop in coercivity coincides with the pinning of moments, which fits with the scenario in which the AFM phase hardens at low temperature—passing through T_B and pinning uncompensated moments while isolating FM clusters. The results allow us to place a rough energy value of $E = k_B(10 \text{ K}) = 0.86 \text{ meV}$ as the crossover above which the FM fluctuations are active.

These observations show an extraordinary correspondence between what is theoretically predicted and experimentally observed across multiple length scales. To further test this, we model the expected effects of iteratively shifting the composite state to lower J and perturb S values on the disordered lattice by increasing the ratio of Mn concentration in the lattice [55]. Analyzing the set of superexchange values used, X-O-Y links containing Mn favor ferromagnetism. Consequently, it is natural to imagine that increasing the relative Mn concentration in the Monte Carlo simulations should eventually lead to global ferromagnetism. Comparative Monte Carlo simulations provide expected spin structure factors as the percentage of Mn increases in relation to the other transition metals populating the lattice, where 20% is equiatomic L5BO (Fig. 5(a)). As % Mn initially increases to 30%, the Néel temperature

decreases, but still $S(0,0,0)$ is negligible and indicates no clear FM order. However, at 40%, the FM signal at $k_{FM}=(0,0,0)$ starts developing and becomes very similar to the AFM signal at $k_{AFM}=(\pi, \pi, \pi)$. This is indicative of a degenerate tipping point between phase preferences. Both signals grow at the same temperature upon cooling. Snapshots of MC simulations visually suggest that the FM clusters have percolated at the 40% Mn concentration, with both the FM and AFM regions being coherent over long distances. At 50% Mn or larger, the AFM $S(k)$ becomes negligible. Increasing Mn to 50% and beyond leads to the FM and AFM states switching roles, with unpercolated AFM clusters being embedded in the fully percolated FM matrix. From this,

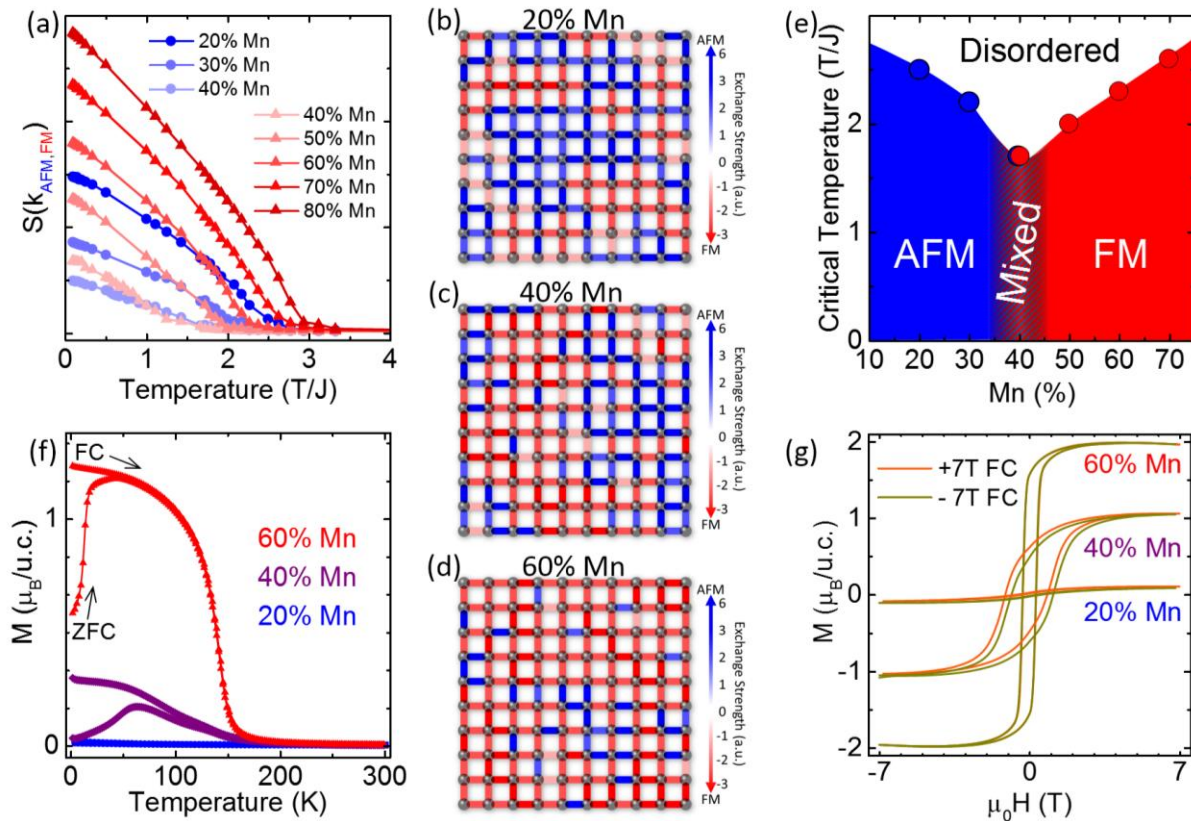


FIG. 5. Predictive modelling and experimental validation of magnetic phase diagram as a function of increasing Mn concentration. (a) Spin structure factor $S(k_{max})$ calculated by varying the % of Mn with the other 4 elements equally distributed in %, where k_{max} is either $(0,0,0)$ (FM, red) or (π,π,π) (AFM, blue) and obtained using Monte Carlo on a $10 \times 10 \times 10$ cluster. At 40% Mn, both AFM and FM orders are percolated in the spin structure, which is why both order parameters are presented in the plot. (b)-(d) Snapshots of calculated $(J S_i \cdot S_j)$ cross-sections for Mn concentrations corresponding to AFM, mixed AFM-FM crossover, and FM regimes show how local AFM (blue), FM (red), and near degenerate (lightly shaded) superexchange values evolve with Mn concentration. (e) The phase diagram derived from the computational model as a function of Mn content. (f) Field cooled and zero field cooled temperature dependent magnetization taken under 1 kOe field for experimentally synthesized films. (g) Magnetization loops taken at 2 K after field cooling under ± 7 T for each of the compositions shows evolution from AFM dominated vertical offset at 20% Mn, to a horizontal exchange bias offset driven by the coexisting percolated AFM/FM phases at 40% Mn, to a FM dominated state at 60% Mn.

we see that it is possible to select and control the dominant percolated magnetic phase, the T_N and T_C of the percolated phases, and that it is even possible to balance the J and S composition in such a way that both AFM and FM can be fully expressed and coexisting as seen in the 40% Mn composition. This can be visualized in example cross sections from the $J(S_i \cdot S_j)$ 10×10 cluster matrices for three different compositions which show the evolution of the superexchange environment moving from percolated AFM at 20% Mn (Fig. 5(b)), to coexisting AFM and FM at 40% Mn (Fig. 5(c)), to percolated FM at 60% Mn (Fig. 5(d)). From these models, a theoretically predicted magnetic phase diagram is compiled (Fig. 5(e)).

Single crystal films of $\text{La}(\text{Cr}_{0.15}\text{Mn}_{0.4}\text{Fe}_{0.15}\text{Co}_{0.15}\text{Ni}_{0.15})\text{O}_3$ (40% Mn) and $\text{La}(\text{Cr}_{0.1}\text{Mn}_{0.6}\text{Fe}_{0.1}\text{Co}_{0.1}\text{Ni}_{0.1})\text{O}_3$ (60% Mn) are synthesized to test these predictions experimentally [55]. In Fig. 5(f), temperature-dependent magnetizations of the synthesized films show that increasing Mn concentration significantly changes the magnetic responses as predicted. At the 60% Mn concentration, the film presents a single sharp upturn in moment consistent with a FM $T_C \approx 160$ K. The 40% Mn composition has a slightly lower critical temperature than the 20% and 60% compositions and a more gradual transition region as would be expected for competing AFM and FM phases. If the local spin and exchange landscape in the synthesized films does mimic the complexity predicted in the model, there should be a high degree of exchange frustration and spin disorder populating these lattices. This would lead to behaviors which may mimic those traditionally observed at the interface of thin film heterostructures comprised of interfacing AFM and FM layers, where intentional design of these exchange interaction discontinuities are used to manipulate exchange bias effects for spin valve, logic, and storage applications [64]. Recent work has shown that increasing the disorder and uncompensated spin populations at the interface of these heterostructures may be the dominating influence in all AFM-FM exchange bias devices [36]. The expectation may then be that the level of spin disorder hosted in the configurationally complex high entropy oxide films should provide outstanding tunability over exchange bias responses even in single crystal monolithic systems.

Exchange bias characterization of the films shows a clear difference in response for each composition (Fig. 5(g)). To understand how these behaviors arise, it is important to consider the shifts in dominant phase energies at each composition. The energy scales involved in the magnetic response of the film are the effective Zeeman energy of the FM (E_F), the anisotropy energy of the AFM (E_{AF}), and the exchange energy at the interface (E_I) between the FM and

AFM components [60]. For a vertical shift, such as that observed in the 20% Mn, to occur from the pinning of FM, it must be that $E_F < E_I$ and $E_F < E_{AF}$, which points to the AFM dominating the magnetic behavior and pinning the FM moments in the film as described above. With increasing Mn concentration, the vertical loop shift observed in the 20% Mn film transitions to a horizontally shifted loop in the 40% Mn film, and finally to a state where field cooling has no obvious effect in the 60% Mn film. Given the observed shift from vertical to horizontal exchange bias response with Mn doping, it is clear that the energy scales shift relative to one another. Horizontal exchange bias implies both $E_I < E_F$ and $E_I < E_{AF}$ and that E_F is strong enough to overcome the exchange energy of the interface and rotate in the biased state [62]. The horizontal shift observed in the 40% Mn film is clear evidence of a traditional exchange biasing phenomenon associated with coexisting and coupled FM and AFM phases of similar energy scale as would be expected in a system with coexisting percolated FM and AFM phases such as that predicted by theory. This control over magnetic coupling in monolithic single phase, single crystal films is remarkable, as the exchange biasing response is usually associated with heterostructured or nanocomposite magnetic materials, where direct coupling is subject to multiple crystalline components. These observations may present an important new direction in understanding the dominating mechanism of exchange bias behaviors more generally. Here, we see that manipulating the local spin disorder can be used to drive exchange bias behaviors in the monolithic single crystal films which resemble responses normally only accessible through intentionally designed heterojunctions; this provides important new insights into recent proposals that spin and exchange disorder can be the dominating factor in generating exchange bias responses [36]. This suggests that the translational symmetry breaking of AFM and FM bonds gives rise to the direct coupling observed in the 40% Mn sample—similarly to that produced in artificial magnetic coupling at heterointerfaces. In the 60% Mn film, there is no longer a percolated AFM phase to bias the dominant FM phase, thus there is no observable loop shift [61]. The unpercolated small FM regions grow and begin to percolate near the region of 40% composition and come to fully dominate for the 60% composition and is also consistent with the observation that the saturation moment approaches the maximum allowed for Mn in $S = 3/2$ state.

III. DISCUSSION AND CONCLUSIONS

Traditional enthalpy-driven synthesis approaches often create materials that possess unintended secondary crystal phase formations or defects which generate extrinsic contributions when more than a few elements are combined. This limits our ability to cover a continuously tunable magnetic parameter phase space that can be simply modelled using only intrinsic parameter variables. The ability to experimentally access narrow regions of calculated parameter space is a critical need to enable computational materials design strategies. The presented work demonstrates that the compositionally disordered but positionally ordered lattices produced using entropy-assisted synthesis approaches may greatly simplify our ability to create materials with very specific macroscopic magnetic responses. A classical Heisenberg model using only the intrinsic spin and exchange parameters is shown to be sufficient to predict the emergence of complex magnetic behaviors and critical temperatures in high entropy oxides comprised of many different magnetically active $3d$ transition metals. Focusing on the transition metal perovskite oxides, we find that the magnetic order parameter can be predicted and synthesized with prediction and experiment matching exceptionally well. Modelling is used to direct elemental compositional ratios required to modify macroscopic expressions of AFM and FM. Shifting composite exchange values through element selection allows us to realize fully percolated AFM and FM order; but also provides guidance to the synthesis of coexisting AFM and FM phases. The ability to design unusual or frustrated competition between two or more states holds a great deal of promise for future exploration.

Manipulating the local degeneracy and frustration may open new possibilities for more complex functionalities. As an example, magnetic frustration has been explored extensively on triangular, pyrochlore, and artificial lattices, where observation of dynamic magnetic behaviors such as spin liquids are generally attributed to degenerate ground states relying on geometric frustration. [65] In magnetically complex high entropy oxides such as those described in this work, it may be possible to replace geometric frustration by exchange frustration controlled by modifying the variance of exchange couplings populating the square lattice. [66–68] Further, the ability to shift local variances in spin and coupling types while maintaining position symmetries may open exciting opportunities for designing novel Griffiths phases or quantum many body systems with tunable critical behaviors [69].

Including quantum fluctuations in the theoretical analysis instead of the classical spins used in the current model, may identify exactly balanced parameters leading to a quantum critical point or, alternatively, to a region of low temperature glassy behavior. Moreover, it is well known that disorder and site-to-site variance in spin and exchange parameters play an important role in nucleating regions of one characteristic or another [59,70,71]. Thus, it is reasonable to predict that manipulating variance while maintaining macroscopic averages may allow for tuning local behaviors that could drive unexpected emergent properties. As an example, considering that the oxides with only two transition metal elements can develop non-collinear states, the true phase diagrams of the compositionally complex systems likely hide more complicated responses than our simple model is able to predict. In a fully percolated phase, controlling the strength and number of randomly distributed frustrating sites into the matrix should reduce the ease with which percolation can occur, and may be utilized to provide exceptional control over transition temperatures. The ability to manipulate the strength and type of coexisting and randomly distributed microstates populating a pristine, well-ordered single crystal offers opportunities to explore the effects of disorder in the strong limit in a system where frustration and degeneracy may lead to unexpected or previously inaccessible phase spaces [72]. By mixing elements having similar magnitude of exchange strength but opposite sign, it may be possible to intentionally design metastability, dynamic responses, and near global frustration into the lattice. With large difference in the site-to-site S and J values, the disorder itself might become a new order parameter as it drives local phase interactions and boundary conditions.

Acknowledgments

Experiment design, sample synthesis, structural characterization, and computational modelling were supported by the US Department of Energy (DOE), Office of Basic Energy Sciences (BES), Materials Sciences and Engineering Division. BLM thanks the Center for Materials Processing, a Center of Excellence at the University of Tennessee, Knoxville funded by the Tennessee Higher Education Commission (THEC), for financial support. This research used resources of the Advanced Photon Source, a U.S. Department of Energy (DOE) Office of Science User Facility operated for the DOE Office of Science by Argonne National Laboratory under Contract No. DE-AC02-06CH11357. A portion of the SQUID magnetometry was performed as a user project at the Center for Nanophase Materials Sciences, which is sponsored at Oak Ridge National Laboratory (ORNL) by the Scientific User Facilities Division, BES, DOE. Some neutron diffraction experiments were conducted at the Spallation Neutron Source, a DOE Office of Science User Facility operated by the Oak Ridge National Laboratory.

References

- [1] V. Baltz, A. Manchon, M. Tsoi, T. Moriyama, T. Ono, and Y. Tserkovnyak, *Antiferromagnetic Spintronics*, Rev. Mod. Phys. **90**, 015005 (2018).
- [2] C. Chappert, A. Fert, and F. N. Van Dau, *The Emergence of Spin Electronics in Data Storage*, Nat. Mater. **6**, 813 (2007).
- [3] R. P. Rairigh, G. Singh-Bhalla, S. Tongay, T. Dhakal, A. Biswas, and A. F. Hebard, *Colossal Magnetocapacitance and Scale-Invariant Dielectric Response in Phase-Separated Manganites*, Nat Phys **3**, 551 (2007).
- [4] B. Gao, T. Chen, D. W. Tam, C.-L. Huang, K. Sasmal, D. T. Adroja, F. Ye, H. Cao, G. Sala, M. B. Stone, C. Baines, J. A. T. Verezhak, H. Hu, J.-H. Chung, X. Xu, S.-W. Cheong, M. Nallaiyan, S. Spagna, M. B. Maple, A. H. Nevidomskyy, E. Morosan, G. Chen, and P. Dai, *Experimental Signatures of a Three-Dimensional Quantum Spin Liquid in Effective Spin-1/2 Ce₂Zr₂O₇ Pyrochlore*, Nat. Phys. **15**, 10 (2019).
- [5] T. Z. Ward, J. D. Budai, Z. Gai, J. Z. Tischler, L. Yin, and J. Shen, *Elastically Driven Anisotropic Percolation in Electronic Phase-Separated Manganites*, Nat Phys **5**, 885 (2009).
- [6] Y.-M. Kim, A. Morozovska, E. Eliseev, M. P. Oxley, R. Mishra, S. M. Selbach, T. Grande, S. T. Pantelides, S. V. Kalinin, and A. Y. Borisevich, *Direct Observation of Ferroelectric Field Effect and Vacancy-Controlled Screening at the BiFeO₃/LaSr_{1-x}MnO₃ Interface*, Nat. Mater. **13**, 1019 (2014).
- [7] H. L. Tuller and S. R. Bishop, *Point Defects in Oxides: Tailoring Materials Through Defect Engineering*, Annu. Rev. Mater. Res. **41**, 369 (2011).
- [8] A. Herklotz, E.-J. Guo, A. T. Wong, T. L. Meyer, S. Dai, T. Z. Ward, H. N. Lee, and M. R. Fitzsimmons, *Reversible Control of Interfacial Magnetism through Ionic-Liquid-Assisted Polarization Switching*, Nano Lett. **17**, 1665 (2017).
- [9] M. S. Lee, R. V. Chopdekar, P. Shafer, E. Arenholz, and Y. Takamura, *Modification of Magnetocrystalline Anisotropy via Ion-Implantation*, AIP Adv. **10**, 045306 (2020).
- [10] R. J. D. Tilley, *Perovskites: Structure-Property Relationships* (Wiley, 2016).
- [11] O. Mustonen, S. Vasala, K. P. Schmidt, E. Sadrollahi, H. C. Walker, I. Terasaki, F. J. Litterst, E. Baggio-Saitovitch, and M. Karppinen, *Tuning the S=1/2 Square-Lattice Antiferromagnet Sr₂Cu(Te_{1-x}W_x)O₆ from Néel Order to Quantum Disorder to Columnar Order*, Phys. Rev. B **98**, 064411 (2018).
- [12] F. Otto, Y. Yang, H. Bei, and E. P. George, *Relative Effects of Enthalpy and Entropy on the Phase Stability of Equiatomic High-Entropy Alloys*, Acta Mater. **61**, 2628 (2013).
- [13] E. P. George, D. Raabe, and R. O. Ritchie, *High-Entropy Alloys*, Nat. Rev. Mater. **4**, 8 (2019).
- [14] N. Dragoë and D. Bérardan, *Order Emerging from Disorder*, Science **366**, 573 (2019).
- [15] C. M. Rost, E. Sachet, T. Borman, A. Moballegh, E. C. Dickey, D. Hou, J. L. Jones, S. Curtarolo, and J.-P. Maria, *Entropy-Stabilized Oxides*, Nat. Commun. **6**, 1 (2015).
- [16] J. L. Braun, C. M. Rost, M. Lim, A. Giri, D. H. Olson, G. N. Kotsonis, G. Stan, D. W. Brenner, J. P. Maria, and P. E. Hopkins, *Charge-Induced Disorder Controls the Thermal Conductivity of Entropy-Stabilized Oxides*, Adv. Mater. **30**, 1805004 (2018).
- [17] Y. Sharma, B. L. Musicó, X. Gao, C. Hua, A. F. May, A. Herklotz, A. Rastogi, D. Mandrus, J. Yan, H. N. Lee, M. F. Chisholm, V. Keppens, and T. Z. Ward, *Single-Crystal High Entropy Perovskite Oxide Epitaxial Films*, Phys. Rev. Mater. **2**, 060404(R) (2018).
- [18] D. Bérardan, S. Franger, A. K. Meena, and N. Dragoë, *Room Temperature Lithium Superionic Conductivity in High Entropy Oxides*, J. Mater. Chem. A **4**, 9536 (2016).
- [19] A. Sarkar, L. Velasco, D. Wang, Q. Wang, G. Talasila, L. de Biasi, C. Kübel, T. Brezesinski, S. S. Bhattacharya, H. Hahn, and B. Breitung, *High Entropy Oxides for Reversible Energy Storage*, Nat. Commun. **9**, 1 (2018).

- [20] S. Zhai, J. Rojas, N. Ahlberg, K. Lim, M. F. Toney, H. Jin, W. C. Chueh, and A. Majumdar, *The Use of Poly-Cation Oxides to Lower the Temperature of Two-Step Thermochemical Water Splitting*, *Energy Environ. Sci.* **11**, 2172 (2018).
- [21] H. Chen, J. Fu, P. Zhang, H. Peng, C. W. Abney, K. Jie, X. Liu, M. Chi, and S. Dai, *Entropy-Stabilized Metal Oxide Solid Solutions as CO Oxidation Catalysts with High-Temperature Stability*, *J. Mater. Chem. A* **6**, 11129 (2018).
- [22] G. N. Kotsonis, P. B. Meisenheimer, L. Miao, J. Roth, B. Wang, P. Shafer, R. Engel-Herbert, N. Alem, J. T. Heron, C. M. Rost, and J.-P. Maria, *Property and Cation Valence Engineering in Entropy-Stabilized Oxide Thin Films*, *Phys. Rev. Mater.* **4**, 100401 (2020).
- [23] W. Zhang, A. R. Mazza, E. Skoropata, D. Mukherjee, B. Musico, J. Zhang, V. M. Keppens, L. Zhang, K. Kisslinger, E. Stavitski, M. Brahlek, J. W. Freeland, P. Lu, and T. Z. Ward, *Applying Configurational Complexity to the 2D Ruddlesden–Popper Crystal Structure*, *ACS Nano* **14**, 13030 (2020).
- [24] R. K. Patel, S. K. Ojha, S. Kumar, A. Saha, P. Mandal, J. W. Freeland, and S. Middey, *Epitaxial Stabilization of Ultra Thin Films of High Entropy Perovskite*, *Appl. Phys. Lett.* **116**, 071601 (2020).
- [25] M. Brahlek, A. R. Mazza, K. C. Pitike, E. Skoropata, J. Lapano, G. Eres, V. R. Cooper, and T. Z. Ward, *Unexpected Crystalline Homogeneity from the Disordered Bond Network in $La(Cr_{0.2}Mn_{0.2}Fe_{0.2}Co_{0.2}Ni_{0.2})O_3$* , *Phys. Rev. Mater.* **4**, 054407 (2020).
- [26] D. B. Miracle and O. N. Senkov, *A Critical Review of High Entropy Alloys and Related Concepts*, *Acta Mater.* **122**, 448 (2017).
- [27] J. Kanamori, *Superexchange Interaction and Symmetry Properties of Electron Orbitals*, *J. Phys. Chem. Solids* **10**, 87 (1959).
- [28] J. B. Goodenough, *Theory of the Role of Covalence in the Perovskite-Type Manganites [$La, M(II)]MnO_3$* , *Phys. Rev.* **100**, 564 (1955).
- [29] J. Zhang, J. Yan, S. Calder, Q. Zheng, M. A. McGuire, D. L. Abernathy, Y. Ren, S. H. Lapidus, K. Page, H. Zheng, J. W. Freeland, J. D. Budai, and R. P. Hermann, *Long-Range Antiferromagnetic Order in a Rocksalt High Entropy Oxide*, *Chem. Mater.* **31**, 3705 (2019).
- [30] M. P. Jimenez-Segura, T. Takayama, D. Bérardan, A. Hoser, M. Reehuis, H. Takagi, and N. Dragoe, *Long-Range Magnetic Ordering in Rocksalt-Type High-Entropy Oxides*, *Appl. Phys. Lett.* **114**, 122401 (2019).
- [31] P. B. Meisenheimer, T. J. Kratochil, and J. T. Heron, *Giant Enhancement of Exchange Coupling in Entropy-Stabilized Oxide Heterostructures*, *Sci. Rep.* **7**, 1 (2017).
- [32] B. Musicó, Q. Wright, T. Z. Ward, A. Grutter, E. Arenholz, D. Gilbert, D. Mandrus, and V. Keppens, *Tunable Magnetic Ordering through Cation Selection in Entropic Spinel Oxides*, *Phys. Rev. Mater.* **3**, 104416 (2019).
- [33] R. Witte, A. Sarkar, R. Kruk, B. Eggert, R. A. Brand, H. Wende, and H. Hahn, *High-Entropy Oxides: An Emerging Prospect for Magnetic Rare-Earth Transition Metal Perovskites*, *Phys. Rev. Mater.* **3**, 034406 (2019).
- [34] Y. Sharma, Q. Zheng, A. R. Mazza, E. Skoropata, T. Heitmann, Z. Gai, B. Musico, P. F. Miceli, B. C. Sales, V. Keppens, M. Brahlek, and T. Z. Ward, *Magnetic Anisotropy in Single-Crystal High-Entropy Perovskite Oxide $La(Cr_{0.2}Mn_{0.2}Fe_{0.2}Co_{0.2}Ni_{0.2})O_3$ Films*, *Phys. Rev. Mater.* **4**, 014404 (2020).
- [35] C. Niu, A. J. Zaddach, A. A. Oni, X. Sang, J. W. Hurt, J. M. LeBeau, C. C. Koch, and D. L. Irving, *Spin-Driven Ordering of Cr in the Equiatomic High Entropy Alloy NiFeCrCo*, *Appl. Phys. Lett.* **106**, 161906 (2015).
- [36] E. Maniv, R. A. Murphy, S. C. Haley, S. Doyle, C. John, A. Maniv, S. K. Ramakrishna, Y.-L. Tang, P. Ercius, R. Ramesh, A. P. Reyes, J. R. Long, and J. G. Analytis, *Exchange Bias Due to Coupling between Coexisting Antiferromagnetic and Spin-Glass Orders*, *Nat. Phys.* **1** (2021).

- [37] P. Peczak, A. M. Ferrenberg, and D. P. Landau, *High-Accuracy Monte Carlo Study of the Three-Dimensional Classical Heisenberg Ferromagnet*, Phys. Rev. B **43**, 6087 (1991).
- [38] M. Eibschütz, S. Shtrikman, and D. Treves, *Mössbauer Studies of Fe 57 in Orthoferrites*, Phys. Rev. **156**, 562 (1967).
- [39] B. Tiwari, A. Dixit, R. Naik, G. Lawes, and M. S. Ramachandra Rao, *Dielectric and Optical Phonon Anomalies near Antiferromagnetic Ordering in LaCrO₃: A Possible near Room Temperature Magnetodielectric System*, Appl. Phys. Lett. **103**, 152906 (2013).
- [40] Y. Murakami, J. P. Hill, D. Gibbs, M. Blume, I. Koyama, M. Tanaka, H. Kawata, T. Arima, Y. Tokura, K. Hirota, and Y. Endoh, *Resonant X-Ray Scattering from Orbital Ordering in LaMnO₃*, Phys. Rev. Lett. **81**, 582 (1998).
- [41] M. A. Korotin, S. Yu. Ezhov, I. V. Solovyev, V. I. Anisimov, D. I. Khomskii, and G. A. Sawatzky, *Intermediate-Spin State and Properties of LaCoO₃*, Phys. Rev. B **54**, 5309 (1996).
- [42] D. Meng, H. Guo, Z. Cui, C. Ma, J. Zhao, J. Lu, H. Xu, Z. Wang, X. Hu, Z. Fu, R. Peng, J. Guo, X. Zhai, G. J. Brown, R. Knize, and Y. Lu, *Strain-Induced High-Temperature Perovskite Ferromagnetic Insulator*, Proc. Natl. Acad. Sci. **115**, 2873 (2018).
- [43] H. Guo, Z. W. Li, L. Zhao, Z. Hu, C. F. Chang, C.-Y. Kuo, W. Schmidt, A. Piovano, T. W. Pi, O. Sobolev, D. I. Khomskii, L. H. Tjeng, and A. C. Komarek, *Antiferromagnetic Correlations in the Metallic Strongly Correlated Transition Metal Oxide LaNiO₃*, Nat. Commun. **9**, 43 (2018).
- [44] K. Ueda, H. Tabata, and T. Kawai, *Atomic Arrangement and Magnetic Properties of LaFeO₃ – LaMnO₃ Artificial Superlattices*, Phys. Rev. B **60**, R12561 (1999).
- [45] K. Ueda, Y. Muraoka, H. Tabata, and T. Kawai, *Atomic Ordering in the LaFe_{0.5}Mn_{0.5}O₃ Solid Solution Film*, Appl. Phys. Lett. **78**, 512 (2001).
- [46] A. K. Azad, A. Mellergård, S.-G. Eriksson, S. A. Ivanov, S. M. Yunus, F. Lindberg, G. Svensson, and R. Mathieu, *Structural and Magnetic Properties of LaFe_{0.5}Cr_{0.5}O₃ Studied by Neutron Diffraction, Electron Diffraction and Magnetometry*, Mater. Res. Bull. **40**, 1633 (2005).
- [47] V. L. J. Joly, P. A. Joy, S. K. Date, and C. S. Gopinath, *Two Ferromagnetic Phases with Different Spin States of Mn and Ni in LaMn_{0.5}Ni_{0.5}O₃*, Phys. Rev. B **65**, 184416 (2002).
- [48] T. Burnus, Z. Hu, H. H. Hsieh, V. L. J. Joly, P. A. Joy, M. W. Haverkort, H. Wu, A. Tanaka, H.-J. Lin, C. T. Chen, and L. H. Tjeng, *Local Electronic Structure and Magnetic Properties of LaMn_{0.5}Co_{0.5}O₃ Studied by x-Ray Absorption and Magnetic Circular Dichroism Spectroscopy*, Phys. Rev. B **77**, 125124 (2008).
- [49] T. Kyômen, R. Yamazaki, and M. Itoh, *Valence and Spin State of Co and Ni Ions and Their Relation to Metallicity and Ferromagnetism in LaCo_{0.5}Ni_{0.5}O₃*, Phys. Rev. B **68**, 104416 (2003).
- [50] V. Solanki, S. Das, S. Kumar, Md. M. Seikh, B. Raveau, and A. K. Kundu, *Crucial Role of Sol–Gel Synthesis in the Structural and Magnetic Properties of LaFe_{0.5}(Co/Ni)_{0.5}O₃ Perovskites*, J. Sol-Gel Sci. Technol. **82**, 536 (2017).
- [51] V. Solanki, Md. Motin Seikh, and A. K. Kundu, *Influence of Chromium in the Structural and Magnetic Properties of LaCo_{0.5}Cr_{0.5}O₃ Perovskite*, J. Magn. Magn. Mater. **469**, 95 (2019).
- [52] M. Gateshki, L. Suescun, S. Kolesnik, J. Mais, K. Świerczek, S. Short, and B. Dabrowski, *Structural, Magnetic and Electronic Properties of LaNi_{0.5}Fe_{0.5}O₃ in the Temperature Range 5–1000K*, J. Solid State Chem. **181**, 1833 (2008).
- [53] D. V. Karpinsky, I. O. Troyanchuk, and V. V. Sikolenko, *Inhomogeneous Magnetic States in Fe and Cr Substituted LaMnO₃*, J. Phys. Condens. Matter **19**, 036220 (2007).
- [54] J. Wang, X. Hao, Y. Xu, Z. Li, N. Zu, Z. Wu, and F. Gao, *Cation Ordering Induced Semiconductor to Half Metal Transition in La₂NiCrO₆*, RSC Adv. **5**, 50913 (2015).
- [55] Materials, methods, and additional text are available as Supplemental Material.
- [56] O. Mustonen, S. Vasala, K. P. Schmidt, E. Sadrollahi, H. C. Walker, I. Terasaki, F. J. Litterst, E. Baggio-Saitovitch, and M. Karppinen, *Tuning the S = 1/2 Square-Lattice Antiferromagnet Sr₂Cu(Te₁ –*

- $x W x$) *O 6 from Néel Order to Quantum Disorder to Columnar Order*, Phys. Rev. B **98**, 064411 (2018).
- [57] F. Parisen Toldin, A. Pelissetto, and E. Vicari, *Strong-Disorder Paramagnetic-Ferromagnetic Fixed Point in the Square-Lattice $\pm J$ Ising Model*, J. Stat. Phys. **135**, 1039 (2009).
- [58] J. Vannimenus and G. Toulouse, *Theory of the Frustration Effect. II. Ising Spins on a Square Lattice*, J. Phys. C Solid State Phys. **10**, L537 (1977).
- [59] J. Burgy, M. Mayr, V. Martin-Mayor, A. Moreo, and E. Dagotto, *Colossal Effects in Transition Metal Oxides Caused by Intrinsic Inhomogeneities*, Phys. Rev. Lett. **87**, 277202 (2001).
- [60] M. Kiwi, *Exchange Bias Theory*, J. Magn. Magn. Mater. **234**, 584 (2001).
- [61] A. N. Dobrynin, D. N. Levlev, K. Temst, P. Lievens, J. Margueritat, J. Gonzalo, C. N. Afonso, S. Q. Zhou, A. Vantomme, E. Piscopiello, and G. Van Tendeloo, *Critical Size for Exchange Bias in Ferromagnetic-Antiferromagnetic Particles*, Appl. Phys. Lett. **87**, 012501 (2005).
- [62] J. Nogués and I. K. Schuller, *Exchange Bias*, J. Magn. Magn. Mater. **192**, 203 (1999).
- [63] J. Nogués, J. Sort, V. Langlais, V. Skumryev, S. Suriñach, J. S. Muñoz, and M. D. Baró, *Exchange Bias in Nanostructures*, Phys. Rep. **422**, 65 (2005).
- [64] H. Ohldag, A. Scholl, F. Nolting, E. Arenholz, S. Maat, A. T. Young, M. Carey, and J. Stöhr, *Correlation between Exchange Bias and Pinned Interfacial Spins*, Phys. Rev. Lett. **91**, 017203 (2003).
- [65] J. Knolle and R. Moessner, *A Field Guide to Spin Liquids*, Annu. Rev. Condens. Matter Phys. **10**, 451 (2019).
- [66] N. Shannon, T. Momoi, and P. Sindzingre, *Nematic Order in Square Lattice Frustrated Ferromagnets*, Phys. Rev. Lett. **96**, 027213 (2006).
- [67] O. Mustonen, S. Vasala, E. Sadrollahi, K. P. Schmidt, C. Baines, H. C. Walker, I. Terasaki, F. J. Litterst, E. Baggio-Saitovitch, and M. Karppinen, *Spin-Liquid-like State in a Spin-1/2 Square-Lattice Antiferromagnet Perovskite Induced by $d 10 - d 0$ Cation Mixing*, Nat. Commun. **9**, 1 (2018).
- [68] L. Liu, H. Shao, Y.-C. Lin, W. Guo, and A. W. Sandvik, *Random-Singlet Phase in Disordered Two-Dimensional Quantum Magnets*, Phys. Rev. X **8**, 041040 (2018).
- [69] T. Vojta, *Disorder in Quantum Many-Body Systems*, Annu. Rev. Condens. Matter Phys. **10**, 233 (2019).
- [70] T. Miao, L. Deng, W. Yang, J. Ni, C. Zheng, J. Etheridge, S. Wang, H. Liu, H. Lin, Y. Yu, Q. Shi, P. Cai, Y. Zhu, T. Yang, X. Zhang, X. Gao, C. Xi, M. Tian, X. Wu, H. Xiang, E. Dagotto, L. Yin, and J. Shen, *Direct Experimental Evidence of Physical Origin of Electronic Phase Separation in Manganites*, Proc. Natl. Acad. Sci. **117**, 7090 (2020).
- [71] H. Lin, H. Liu, L. Lin, S. Dong, H. Chen, Y. Bai, T. Miao, Y. Yu, W. Yu, J. Tang, Y. Zhu, Y. Kou, J. Niu, Z. Cheng, J. Xiao, W. Wang, E. Dagotto, L. Yin, and J. Shen, *Unexpected Intermediate State Photoinduced in the Metal-Insulator Transition of Submicrometer Phase-Separated Manganites*, Phys. Rev. Lett. **120**, 267202 (2018).
- [72] A. Simonov and A. L. Goodwin, *Designing Disorder into Crystalline Materials*, Nat. Rev. Chem. **4**, 12 (2020).